`Vol. 4, No. 5, pp. 430-454, (December 2023)
DOI: **10.21608/aujes.2023.221708.1173**
Aswan University Journal of Environmental Studies (AUJES)
Online ISSN: 2735-4237, Print ISSN: 2735-4229
Journal homepage: https://aujes.journals.ekb.eg/ E-mail: AUJES@aswu.edu.eg
Original research

Concentration Effect of MoO_3 doping SnO_2 on the physical properties of thin films for use as environmentally friendly energy storage materials.

F.M. Abelwahab[a,b], A. A.Elamina[a,b] ,M.M.Sammer[a], A. M. Badr[a,b]

[a] *Department of Physics, Faculty of Science, Aswan University, Aswan, Egypt*
[b] *Research Center for Nano Materials Studies and their Promising Technologies, Aswan, Egypt*

Received: 8/7/2023 Accepted: 30/9/2023

Abstract:

Spin-coating deposited transparent conducting MoO_3 doped SnO_2 thin films. MoO_3 (0 ,7,10,12 and 15 wt.%) doped SnO_2 thin films spin-coating deposited onto glass substrates at 550℃ were studied for their structural, optical and temperature dependent electrical behaviors. X-ray diffraction patterns revealed a tetragonal phase with polycrystalline structure. The XRD results confirmed decrease in crystallite size with increasing the MoO_3 doping content. SEM was used to analysis of thin films revealed decreasing in spherical particle size. The samples 'Composition has been analyzed using EDX. The UV-VIS-NIR spectroscopic investigation showed a reduction in visible optical transmission in addition to a significant decrease ten increase in optical bandgap by increasing MoO_3 doping contents. Activation energy was calculated from temperature dependent electrical resistivity data measured in the range 370 to 460 K. The current showed that MoO_3 doped SnO_2 thin films are an attractive option for IR coating ,solar cells and other optoelectronic applications.

Keywords: MoO_3 doped SnO_2; spin coating; thin film; optical properties; dc conductivity.

1- Introduction

Transparent conducting oxides (TCOs) have received a lot of attention in research because they have a high transmittance in the visible range and also good electrical conductivity [Ali et al., 2017). These properties enable TCOs to be used with a wide variety in several applications such as photo catalysis, laser diodes and light-emitting diodes (LEDs) (Park et al.,2006), electro catalysis (Zhang et al.,2015), gas sensors (Alenezi et al., 2014), electroluminescent devices (Lu et al,2014), photovoltaics, and energy-efficient windows (Krishnapriya et al.,2015). Metal oxides, particularly those of In, Sn and Zn have been used to synthesis a very common transparent coatings (Kaplan et al., 1995). Accordingly, tin oxide (SnO_2) has been considered as the most significant metal oxide semiconductor with a wide bandgap and n-type conductivity. The rutile SnO_2 has a tetragonal crystal structure, with two tin and four oxygen atoms per unit cell. SnO_2 has attracted much attention because of unique physical properties such as high optical transparency in the visible region, low electrical resistance, and excellent chemical and thermal stability (Alinauskas et al., 2017).

Corresponding author*: E-mail address: aaelamin2000@yahoo.com

These unique properties of SnO_2 can be enhanced either by improving both the particle size and the specific surface area (Pan et al, 2007) and (Sun et al., 2006) or by doping with other metal oxide having a major influence on its chemical and physical properties (Wen et al., 2007; Choi et al., 2008). However, the electrical resistivity of tin dioxide increases in air by approximately two order of magnitude by introducing MoO_3 into the SnO_2's lattice, which may be due to electrons transfer from oxygen vacancies to Mo^{6+} (Arbiol et al., 2006). SnO_2 thin films have been synthesized by several techniques including pulsed laser deposition, chemical vapor deposition, spray pyrolysis, sol-gel process, the DC sputtering etc. (Bouaine et al., 2007; Fan et al., 2014; Chao et al., 2010). Amongst all, sol-gel technique followed by spin coating is regarded as one of the best techniques because of low cost and simplicity of the deposition processes (Arif et al., 2018).

In the current work, synthesis of un-doped SnO_2 and MoO_3 doped SnO_2 with various concertation (0, 7, 10, 12 and15) wt. % by sol-gel spin coating technique. The current work is mainly aimed to assess the influence of the dopant concentration on the structural, optical, and electrical properties for un-doped SnO_2 and MoO_3 doped SnO_2 thin films. Additionally, the optoelectronic properties were also investigated for the film samples.

2. Materials and Methods

2.1 Precursor Materials, Spin-coating Parameters and Coating Procedure

Pure and MoO_3-doped SnO_2 thin films were deposited on glass substrates using a spin-coating technique. Stannous chloride ($SnCl_2.2H_2O$, purity 99.999 %) was used as a starting material for preparing the base precursor solution, whereas 5.0 g of tin (II) chloride dehydrate was dissolved in 2.5 ml of concentrated hydrochloric acid (HCl 37 %, purity 99.999 %). This reactant solution was magnetically stirred at 90 °C for 15 minutes using Thermo Scientific Hotplate Stirrer (Model-SP88857105), and then the resulting solution was diluted by adding methanol up to 12.5 ml under continuous stirring with turning the heat off that allows the solution to naturally cool down to room temperature. This step was followed by ageing for 24 h, and thereafter a homogenous clear solution was obtained and denoted as A, which was used as the base precursor solution.

Ammonium heptamolybdate tetrahydrate AHM ($(NH_4)6Mo_7O_{24}.4H_2O$, 99.999) was used as a starting material for preparing four distinctable dopant precursor solutions with different concentrations, whereas 0.35, 0.51, 0.60 and 0.74 g of AHM was consecutively dissolved in 60 ml of deionized (DI) water having 18.2 MΩ·cm electrical resistivity of at 25 ºC (the DI was withdrawn from Barnstead™ Smart2Pure™ Water Purification System). Such a reactant solution was vigorously stirred at 500 rpm for 20 min, and thereafter a homogenous clear solution was obtained. The resulting solutions were used as four distinctable dopant solutions and denoted as B1, B2, B3 and B4, respectively. These solutions were consecutively mixed with solution A under vigorous stirring at 500 rpm for 30 min, resulting in four mixtures with different weight percentages of [AHM]/[Stannous chloride] ratio that were denoted as C1 (Solution of 7.0 wt.% MoO_3), C2 (Solution of 10 wt.% MoO_3), C3 (Solution of 12 wt.% MoO_3) and C4 (Solution of 15 wt.% MoO_3), respectively. These mixtures were utilized as precursor solutions in depositing pure and MoO_3-doped SnO_2 thin films on cleaned 20 x 20 mm^2 glass substrates using a VTC-100 Vacuum Spin Coater. To obtain uniform and well adherent coatings on the substrates, such a glass substrate was preheated at 180 ºC for 10 minutes before using in spin coating processes. Firstly, solution A was dispensed from glass syringe onto glass substrate for preparing the un-doped tin dioxide (TDO) thin film, and then the substrate spun throughout the first stage to spread out the solution evenly across the substrate.

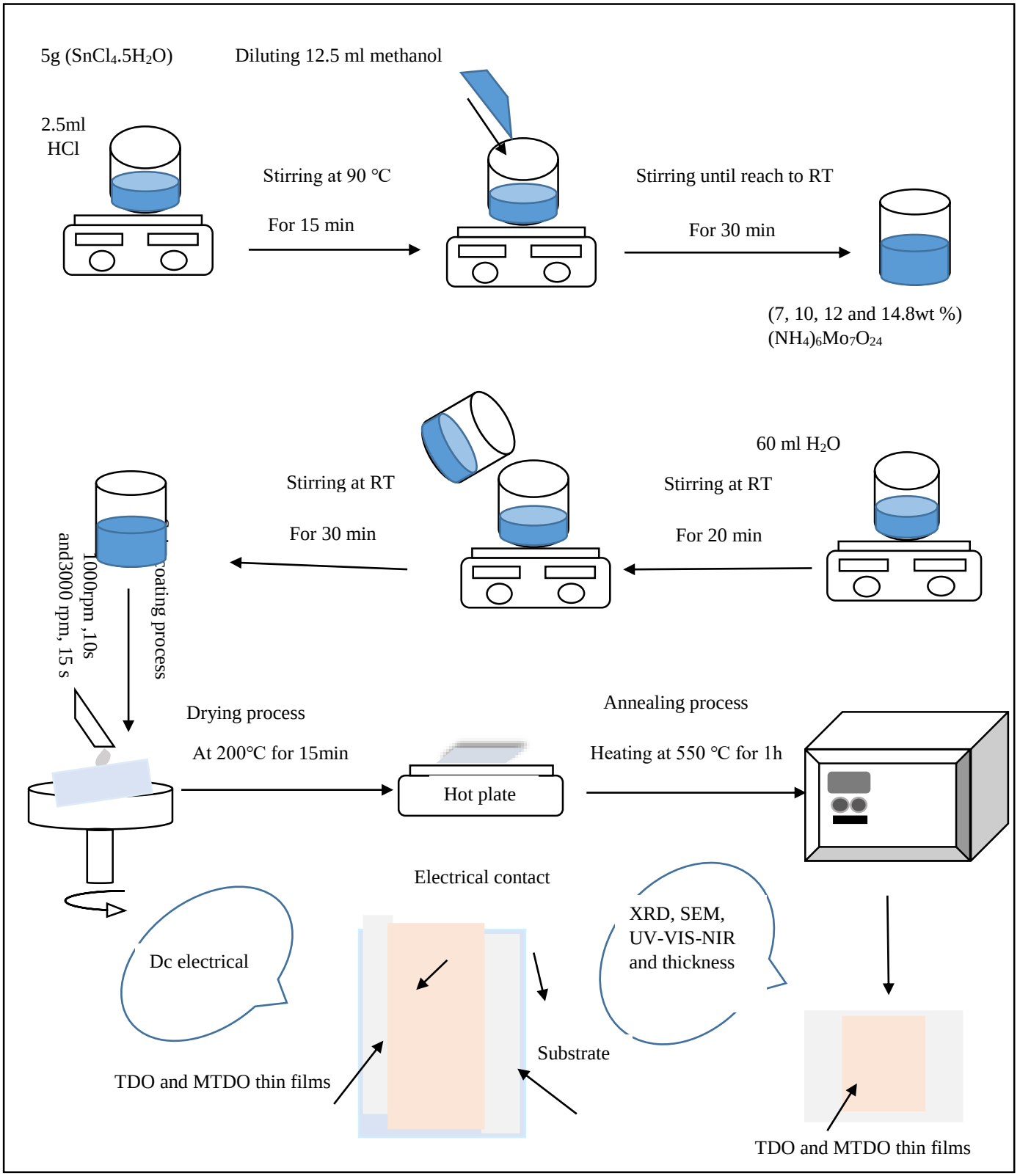

Figure 1. Schematic representing of synthesis and characterization of pure and MoO_3-doped SnO_2 thin films.

The spin speed (SPD1) and the spin time (t1) of this stage were pre-set at 1000 rpm and 10 s, respectively. The first stage was followed automatically by the high-speed spinning stage (second stage) to coat the substrate uniformly, however the spin speed (SPD2) and the spin time (t2) of the second stage were pre-set at 3000 rpm and 15 s, respectively. Thereafter, the coated substrate was dried at 200 ºC for 30 minutes to evaporate the solvent and to remove organic residuals. The experimental procedures from coating to drying were repeated for only 5 times, whereas this number of coating cycles ensures the optimum number of layers satisfying betterment in the transparency and the electrical conductivity of the produced film. The resulting thin film was thermally treated at 550 ºC for 1 hours with a heating/cooling rate of 5 °C/min. All the above-mentioned coating processes were repeated consecutively using solutions C1, C2, C3 and C4 for preparing four additional thin films coded as MTDO1 (7.0 wt.% MoO_3), $MTDO_2$ (10.0 wt.% MoO_3), $MTDO_3$ (12.0 wt.% MoO_3) and MTDO4 (15.0 wt.% MoO_3), respectively. The thickness measurements were carried out for the thin films under investigation using Model–P7 Stylus Profilometer (KLA-Tencor, USA), however such a film sample was pressed by a constant applied force of 2 mg over a scan length of 2000 µm with a speed of 100 µm/s and a sampling rate of 50 Hz is shown in figure 1.

2.2 Sample Elaboration and Instrumentations

2.2.1. X-Ray Diffraction (XRD)

The phase identification and crystal structure evolution of the resulting thin films were analyzed by using an X-ray diffractometer (PANalytical X'Pert Pro) at room temperature with Cu-Kα1 radiation source (1.54056 Å) wavelength a. The obtained XRD profiles were measured in the 2θ range from 10° to 70°, with a step of 0.02° and scanning rate of 2.5° min^{-1}.

2.2.2. The scanning electron microscopy (SEM) micrograph

The resultant un-doped SnO_2 and MoO_3-doped SnO_2 thin films were also measured using a QUANTA FEG- 250 (ESEM) scanning electron microscope at accelerating voltage of 30 kV, to get plenty resolution with minimal radiation damage to the composition. And using an EDAX ELEMENT energy dispersive X-ray spectrometer with resolution of 128 eV, to get chemical composition.

2.2.3. Transmission Spectroscopy

The spin deposited thin films were characterized using a UV-VIS-NIR JASCO spectrophotometer model V-670. Transmission spectra were performed at room temperature in the spectral range 190–2700 nm, with a wavelength scanning speed of 400 nm min^{-1} and a data interval of 5 nm for all the thin film samples investigated here.

2.2.4. Electrical Measurements

For all un-doped SnO_2 and MoO_3-doped SnO_2 thin films, The DC electrical measurements were carried out to a thin film under study at temperatures ranges that varied from 370 to 460K with an interval of 5.0K by applying 8.0V bias voltage. Silver paste was used to make Contacts between the thin film and the metal electrodes, The Keithley 6517B Instrument, which has a 10^{-15} A operating sensitivity, was used to assist in the electrical measurements. The 6517B Electrometer features a built-in V-Source, with the 100 V range providing up to ±100 V at 10 mA and the 1000 V range providing up to ±1000 V at 1 mA, and measurement capabilities for resistance and resistivity measurements (surface or volume resistivity) ranging from 10 Ω to 210 PΩ. furthermore, the '6517 Hi-R Temp and RH' program software

was utilized, which enables for highly exact resistance/ resistivity measurements to be taken at the same time as temperature (T) and relative humidity (RH) observations. When using the Alternating Polarity Test method, the electrometer's Voltage Source output of the switches between two voltages ('V Offset + V Alternating' and 'V Offset – V Alternating') at timed intervals. A well-grounded power outlet of 0.5 Ω was used to accomplish these tests with high accuracy and realization, and grounding wires were safely attached to the instruments and components from this outlet. A schematic representing of synthesis and characterization of pure and MoO_3-doped SnO_2 thin films.

3. RESULTS AND DISCUSSION

3.1. Structure Identification and Evolution

The structural properties of the spin-coated TDO and MTDO thin films were investigated using an x-ray diffraction technique. The structures of the produced thin films were identified based on the measured diffraction patterns, and then the evolution of such exhibited structure was explored and analyzed. Figure 2 illustrates the measured XRD patterns of these MTDO film samples, and it also depicts the diffraction pattern measured for the TDO (i.e. un-doped SnO_2) thin film.

Figure 2a shows the measured XRD pattern of the TDO thin film that exhibits a series of four predominant diffraction peaks observed at 2θ = 26.47º, 33.83º, 37.81º and 51.77 º alongside with six low intensities peaks observed at 2θ = 38.93º, 42.55º, 61.93º, 62.45º, 64.73º and 65.95º. Both the predominant and the low intensities peaks are well matched with the standard reference pattern given by the JCPDS Card Nos. 00-041-1445, revealing the formation of a rutile tetragonal SnO_2 structure. accordingly, these diffraction peaks are assigned to the (110), (101), (200), (211), (111), (210), (310), (221), (112), (301) crystallographic planes, respectively. Figure 2a revealed that the comparatively intensive peaks at 26.47º, 33.83º and 51.77º assure the preferential orientation growth along the (110), (101) and (211) planes for the TDO film sample.

By incorporating 07.0 wt% MoO_3-doping content into the SnO_2 lattice, the diffraction peaks matched with the tetragonal SnO_2 structure were reduced to be four distinguishable peaks that are the more intense peaks assigned to the (110), (101) and (211) crystallographic planes in addition to a weak diffraction peak assigned to the (301) plane as inferred from Figure 2b. These three more intense peaks remain clearly the dominant ones within the MTDO1's pattern, suggesting that the incorporation of dopant ions in the SnO_2 lattice does not change the tetragonal SnO_2 structure.

Based on Figure 2b, the MTDO1's diffraction pattern exhibits additional five clear peaks observed at 12.69º, 23.49º, 25.63º, 33.19º and 34.33º alongside with a low intensity peak observed at 57.53º, indicating the coexistence of the thermodynamically stable phase of MoO_3 (i.e. orthorhombic structure), whereas these peaks are indexed to the standard reference pattern given in the JCPDS Card Nos. 00-005-0508 and can be assigned to the (020), (110), (040), (101), (140) and (171) planes, respectively.

In view of Figure 2b, the MTDO1's pattern shows three well defined peaks observed at 28.85º, 41.41º and 63.59º accompanied with two weak diffraction peaks observed at 64.51º and 65.65º, reflecting the coexistence of the metastable phase of MoO_3 (i.e. monoclinic structure), however these peaks are well matched with the standard reference pattern given in the JCPDS Card Nos. 00-084-1360 and can be assigned to the (112), (222), (431), (151) and (025) planes, respectively.

By the increase in the MoO_3-doping content from 07.0 to 10.0 wt%, Figure 2c revealed that the MTDO2's diffraction pattern exhibits a new well defined peak observed at 16.63º alongside with an additional low intensity peak observed at 48.49º. These peaks matches well with the orthorhombic MoO_3 structure and can be assigned to the (011) and (040) planes, respectively.

Moreover, no new distinguishable peaks were observed by further increase in the MoO_3-doping content from 10.0 to 15.0 wt% as inferred from the diffraction patterns of the MTDO3 and MTDO4 film samples (Figures 2d and e), while these patterns exhibit a slight decrease in the peaks' heights by increasing the doping content.

Figure 2 also revealed that an abrupt decrease in the peaks' heights was observed by introducing 07.0 wt% MoO_3 into the SnO_2 lattice, suggesting significant lower growth rate of the progressive nucleation accompanied with the onset of a mixed phase comprised of tetragonal-SnO_2, orthorhombic- and monoclinic-MoO_3 phases (Figure 2a, b). Nevertheless, an appreciable decrease in peaks' heights was observed by increasing the MoO_3-doping content as inferred from Figures 2b-e, indicating weaker crystallinity and smaller crystallite size for such a film sample having larger amount of MoO_3.

By inspecting Figure 2, the more intense peaks matched with the tetragonal SnO_2 structure and assigned to the (110), (101) and (211) crystallographic planes remain the dominant ones within the XRD patterns of all the MoO_3-doped SnO_2 film samples. The dominance of these diffraction peaks suggests complete incorporation of the MoO_3-doping contents, implying that the dopant ions substitute normal positions in the SnO_2 lattice, and thereby the tetragonal SnO_2 structure have no significant change due to the MoO_3-doping processes. These observations are well consistent with what have been previously reported by (Ivanovskaya et al.,2001).

Based on the more intense peaks that are indexed to the tetragonal SnO_2 structure and assigned to the (110), (101) and (211) crystallographic planes, the average values of the lattice parameters were calculated for all the produced film samples using the following formulas:

$$\mathbf{1}/d_{hkl}^2 = \mathbf{((}h^2 + k^2\mathbf{)}/a^2\mathbf{)} + \mathbf{(}l^2/c^2\mathbf{)}$$

$$Sin^2\boldsymbol{\theta} = \mathbf{(}\lambda^2\mathbf{/4) [((}h^2 + k^2\mathbf{)}/a^2\mathbf{)} + \mathbf{(}l^2/c^2\mathbf{)]} \qquad \mathbf{(1)}$$

Where, h, k, and l are Miller indices of reflector planes appearing on the diffraction spectrum, d_{hkl} is the interplanar spacing of the (hkl) plane. The calculated lattice parameters of the film samples are compiled in the summary Table 1. These values are in good agreement with the standard values given in the JCPDS Card Nos. 00-041-1445 (a = 4.7382 Å, c = 3.1871 Å and c/a = 0.6726), however no appreciable changes in the lattice parameters were observed by increasing the MoO_3-doping content as inferred from Table 1.

The mean crystalline size of such produced thin film was also evaluated based on the more intense peaks that are indexed to the tetragonal SnO_2 structure and assigned to the (110), (101) and (211) crystallographic planes. Scherrer's Equation was used in evaluating the mean crystalline size of each film sample (Cullity and Stock, 2001):

$$D_{hkl} = \mathbf{(}k\lambda_{CuK\alpha}\mathbf{)/ (\beta cos\theta)} \qquad \mathbf{(2)}$$

where D is the average crystallite size perpendicular to the diffracting plane (hkl), k is the shape factor (assuming that the particles are spherical, k = 0.89), $\lambda_{CuK\alpha}$ is the wavelength of the incident x-ray beam (1.54056 Å), β is the full width at half maximum of more intense

diffraction peak corrected for instrumental line broadening (rad), and θ is the Bragg angle of diffraction (rad).

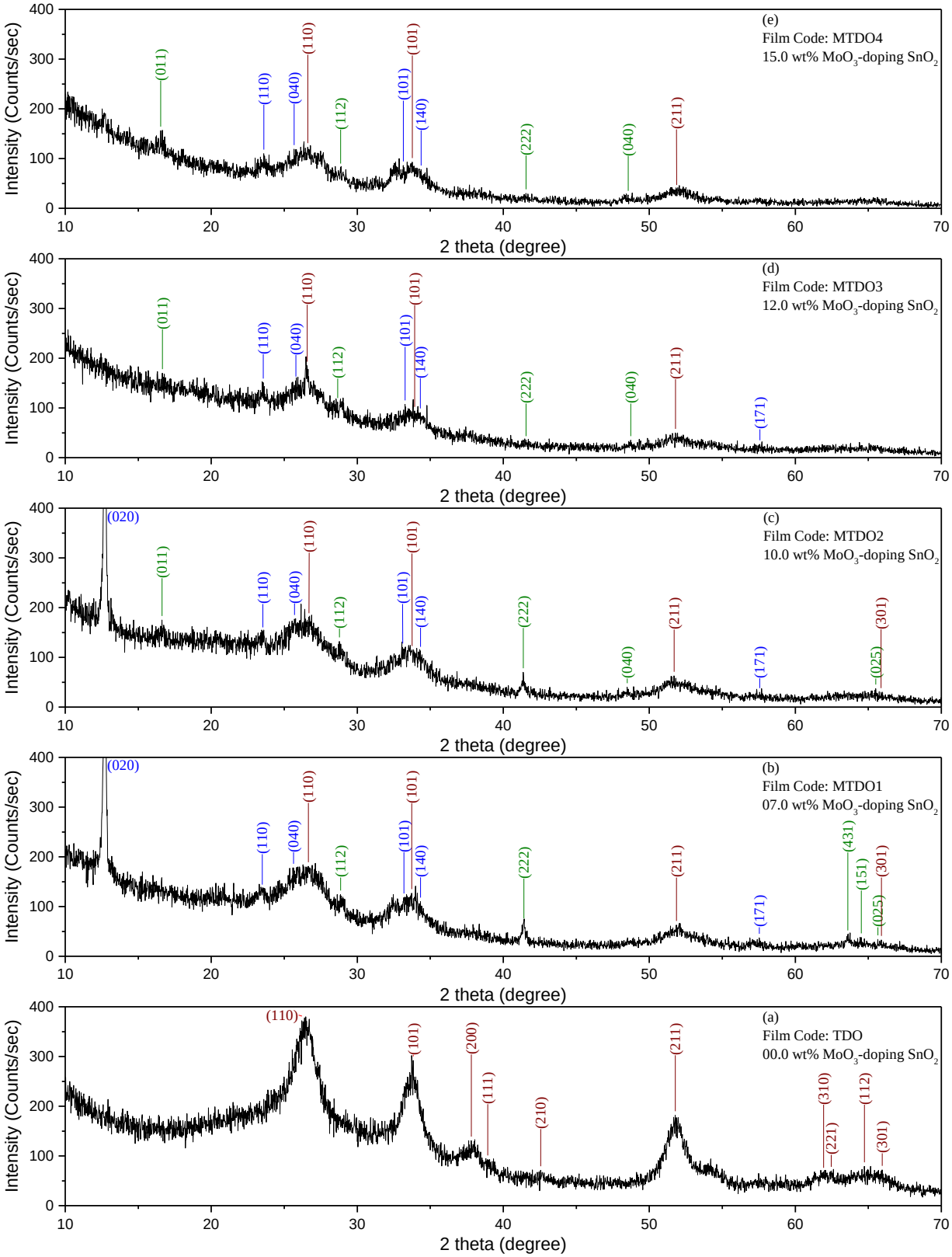

Figure 2. XRD patterns of pure and MoO_3 doped SnO_2 thin films deposited at 550°C with spin coating.

Table 1. The structural parameters of the spin-coated TDO and MTDO thin films compared to those given in the standard reference pattern of rutile tetragonal SnO2 structure (JCPDS Card Nos. 00-041-1445)

Film Code	Experimental						Standard (JCPDS Card Nos. 00-041-1445)			
	Peak Position Degree	d-Spacing Å	Lattice Parameters a (Å)	c (Å)	c/a (Å)	Crystallite Size CS (nm)	d-Spacing Å	Miller Indices h	k	l
TDO	26.47	3.3645	4.748	3.171	0.667	74.83	3.3470	1	1	0
	33.83	2.6474					2.6427	1	0	1
	51.77	1.7644					1.7641	2	1	1
MTDO1	26.65	3.3422	4.720	3.199	0.677	48.42	3.3470	1	1	0
	33.73	2.6551					2.6427	1	0	1
	51.85	1.7619					1.7641	2	1	1
MTDO2	26.69	3.3372	4.726	3.219	0.681	40.34	3.3470	1	1	0
	33.75	2.6535					2.6427	1	0	1
	51.69	1.7669					1.7641	2	1	1
MTDO3	26.57	3.3520	4.741	3.178	0.670	32.01	3.3470	1	1	0
	33.93	2.6399					2.6427	1	0	1
	51.79	1.7638					1.7641	2	1	1
MTDO4	26.61	3.3471	4.724	3.188	0.674	21.63	3.3470	1	1	0
	33.77	2.6520					2.6427	1	0	1
	51.87	1.7612					1.7641	2	1	1

JCPDS Card Nos. 00-041-1445: a = 4.7382 Å; c = 3.1871 Å; c/a = 0.6726

Based on data recorded in Table 1, the mean crystallite size significantly decreases by introducing 07.0 wt% MoO_3 into the TDO (pure tin dioxide) lattice that evidenced through the values of the crystallite size for the TDO and MTDO1 film samples that were found to be ~ 74.83 nm and ~ 48.42 nm, respectively. Nevertheless, the mean crystallite size was found to be slightly decreased by increasing the MoO_3-doping content down to ~ 21.63 nm for the MTDO4 film sample (see Table 1). Otherwise, (Zampiceni et al., 2002) have reported that the crystallite sizes evenly decrease by increasing the MoO_3-doping content.

3.2. Morphological Features and Particle Size Analysis by SEM

The surface morphology of MoO_3 (0 to 15 wt. %) doped SnO_2 thin films are investigated by scanning electron microscopic, which is shown in figure. The surface of the un-doped SnO_2 and MoO_3-doped SnO_2 thin films (Figure 3a, c, and e) contain uniform distribution of spherical shaped particles and fewer voids. When dopant concentration increases to 12 and 15 wt. % (Figure 3g, i) form agglomeration of smaller grains in thin films. These are reason for the increment dopant concentration of MoO_3 present in SnO_2 film samples.

The enhancement variance in thin film shape can be related to modest differences in deposition circumstances as well as differences in precursor concentration, which results in the alter in total flow of molecules extending the substrate and so modifying the nucleation and growth process (Givargizov ., 2013).

The Image J software evaluate the particle diameters of un-doped SnO_2 and MoO_3-doped SnO_2 thin films. (Figure 3b, d, f, h and j) exhibit data in the form of histogram particle size distribution in the film samples analyzed. The particle size decreases with increasing doping concentration from 25.5 nm for TDO thin film to 9.9 nm for MTDO04 film. Energy dispersive X-ray spectroscopy (EDX) analysis was performed to verify the chemical composition of our thin films. Figure 4 depicts the EDX spectra of pure SnO_2 and MoO_3-doped SnO_2 films.

The existence of Sn and O elements in pure SnO_2 and Sn, O and Mo in doped SnO_2 thin films is confirmed by EDX data and its Wt. % and at. % ratio increases while increasing the doping

concentration. In addition, the silicon (Si) peak is observed which might be resulted from the glass substrate.

3.3. OPTICAL PROPERTIES

Figure 5a depicts the Optical transmittance spectra of un-doped SnO_2 and MoO_3-doped SnO_2 thin films measured at wavelengths ranging from 190 to 2700 nm. Figure 5a clearly illustrates that the spectral dependence of the transmission reveals a typical behavior across the entire investigated range of the incident photon energy for the thin film samples deposited with varying concentrations of MoO_3. The high average transmittance in visible region belongs to un-doped SnO_2 thin film. The average transmittance of the MoO_3 doped SnO_2 films decreases with the increasing MoO_3 doping concentration. However, at visible wavelengths, the average transmittance of un-doped SnO_2 of 93.65–96.88% decrease to transmittance range of 83.12–90.99% with 7wt. % MoO_3 doping ratio. When MoO_3 doping ratio is increased more, the transmittance values of 80.55–88.55% for 15Wt. % MoO_3 doped sample. These values are comparable to those previously reported in various studies (El Radaf et al., 2019) and (Mazloom and Ghodsi, 2013). According to these values, all TDO and MTDO thin films have good optical transparency in the visible region, whereas the TCO applications require at least 80 % optical transparency (Turgut and Sönmez, 2014) and (Turgut et al., 2014).

The TDO and MTDO film samples have great potentials for applications in optoelectronic devices such as solar cells and IR coating windows (Ravichandran et al., 2013) and (Ahmed et al., 2006) due to their relatively high optical transparency in the visible region and near-infrared region (~500 – 800 nm). The increase in MoO_3 doping concentration can be attributed to an increase in scattering center (grain boundaries, defects…) within XRD results in smaller grain size as well as concurrent enhancement of lattice distortion and surface roughness. This is the main reason for decreasing the optical transmission by increasing the MoO_3 doping percentage as noticed in the XRD results. These results are supported with those made previously by (Soitah et al., 2010), (Liu et al., 2011) and (Ibrahim et al., 2013).

According to the inference made from the Figure 5a, a fundamental absorption edge at a specific wavelength was noticed for a film sample of this type at particular wavelength. This is an optical absorption threshold, which is the threshold for charge transition between the highest valance band state and the lowest conduction band state. The absorption edge in the present study shows a shift toward shorter wavelength, confirming the impact of raising the MoO_3 doping percentage.

In contrast, for un-doped SnO_2 thin film, the optical transmission measurements revealed a shoulder near to 285 nm, which refers to the absorption edge for TDO thin film, as shown in Figure 5a.

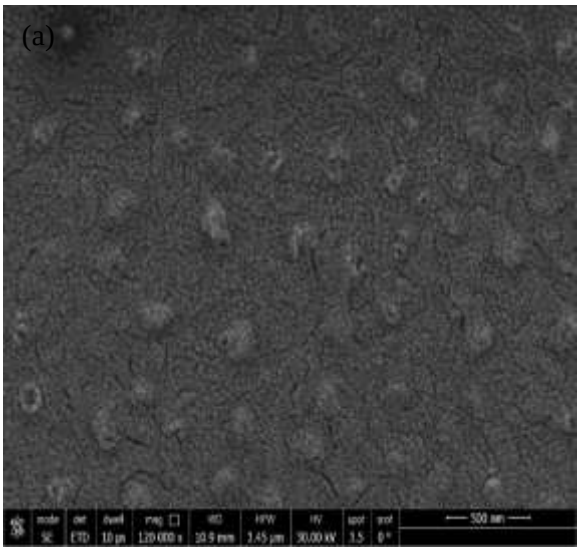
(a)

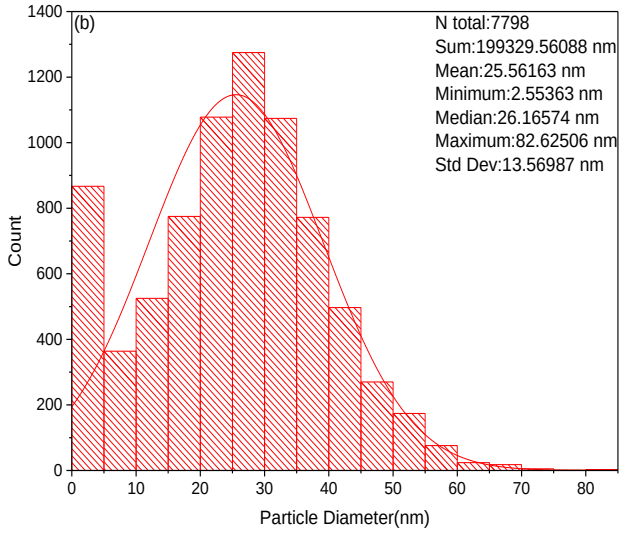
(b)
N total:7798
Sum:199329.56088 nm
Mean:25.56163 nm
Minimum:2.55363 nm
Median:26.16574 nm
Maximum:82.62506 nm
Std Dev:13.56987 nm
Count
Particle Diameter(nm)

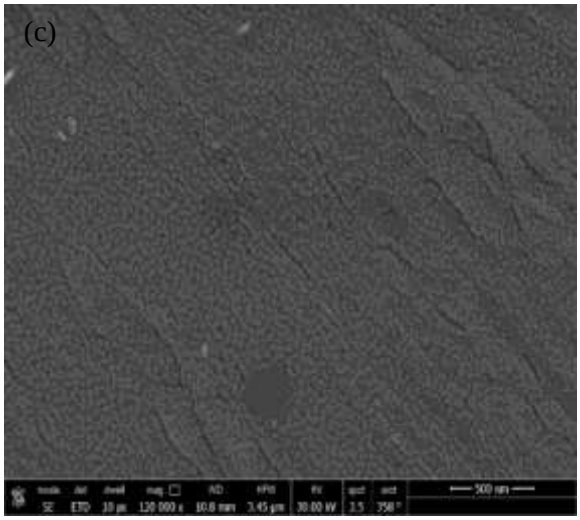
(c)

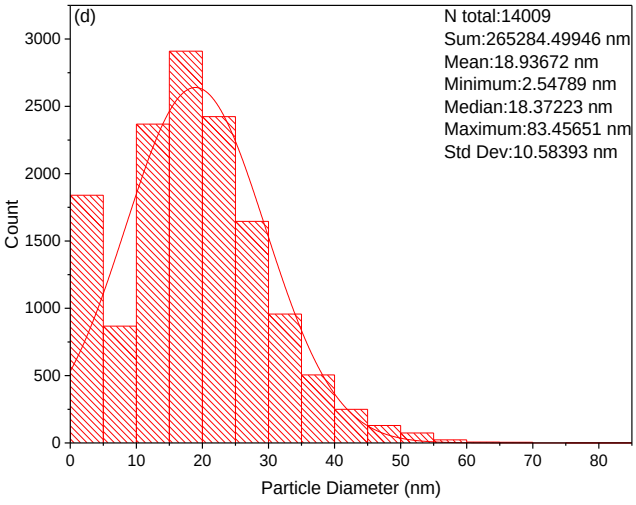
(d)
N total:14009
Sum:265284.49946 nm
Mean:18.93672 nm
Minimum:2.54789 nm
Median:18.37223 nm
Maximum:83.45651 nm
Std Dev:10.58393 nm
Count
Particle Diameter (nm)

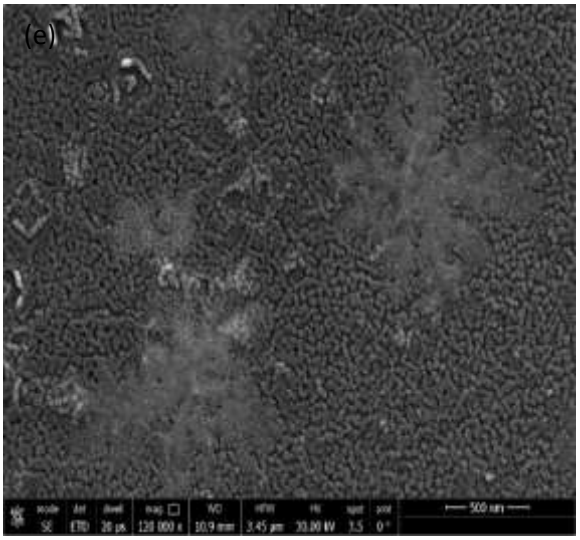
(e)

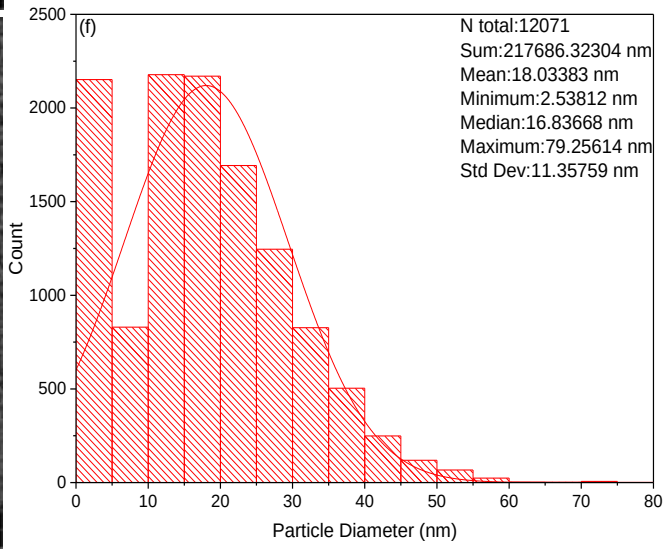
(f)
N total:12071
Sum:217686.32304 nm
Mean:18.03383 nm
Minimum:2.53812 nm
Median:16.83668 nm
Maximum:79.25614 nm
Std Dev:11.35759 nm
Count
Particle Diameter (nm)

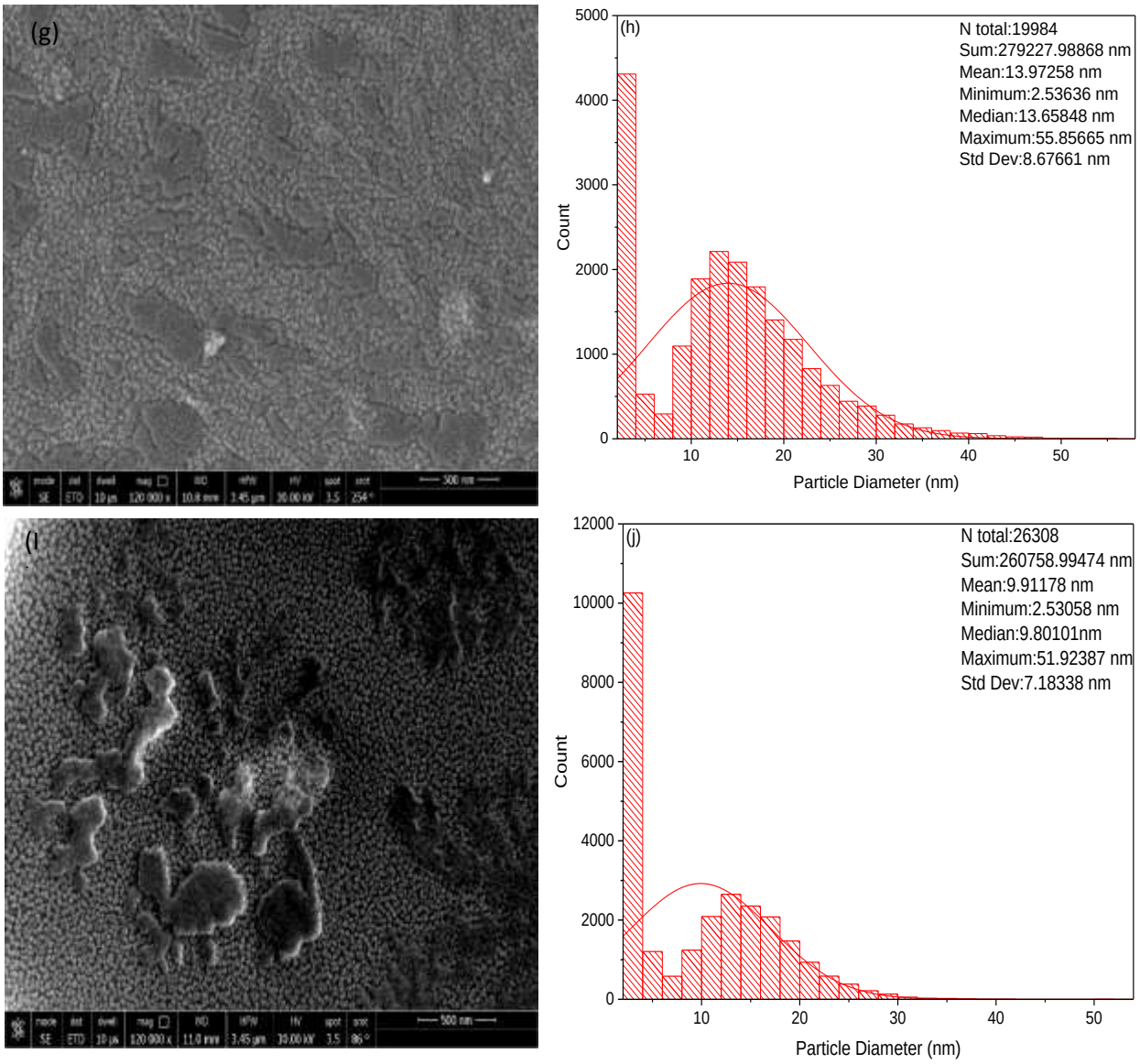

Figure 3. SEM micrograph and histogram of corresponding particle size distribution of pure and MoO_3 doped SnO_2.

(a)

Element	Wt. %	At. %	Error %
O K	34.96	50.24	9.65
Si K	59.14	48.41	2.92
Mo L	4.44	1.06	12.64
Sn L	1.46	0.28	6.49

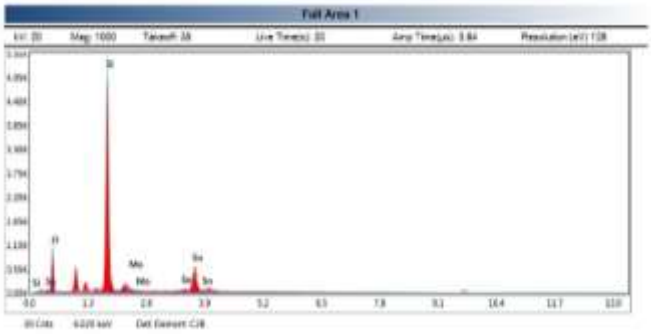

(b)

Element	Wt. %	At. %	Error %
O K	42.08	90.6	9.39
Si K	45.08	36.56	3.48
Mo L	9.83	2.34	6.53
Sn L	2.54	0.49	7.83

(c)

Element	Wt. %	At. %	Error %
O K	30.48	48.78	10.42
Si K	51.2	46.65	3.45
Mo L	12.45	3.32	7.27
Sn L	5.87	1.27	6.32

(d)

Element	Wt. %	At. %	Error %
O K	16.36	44.18	10.42
Si K	20.65	31.72	5.94
Mo L	14.01	6.3	4.94
Sn L	48.96	17.6	2.62

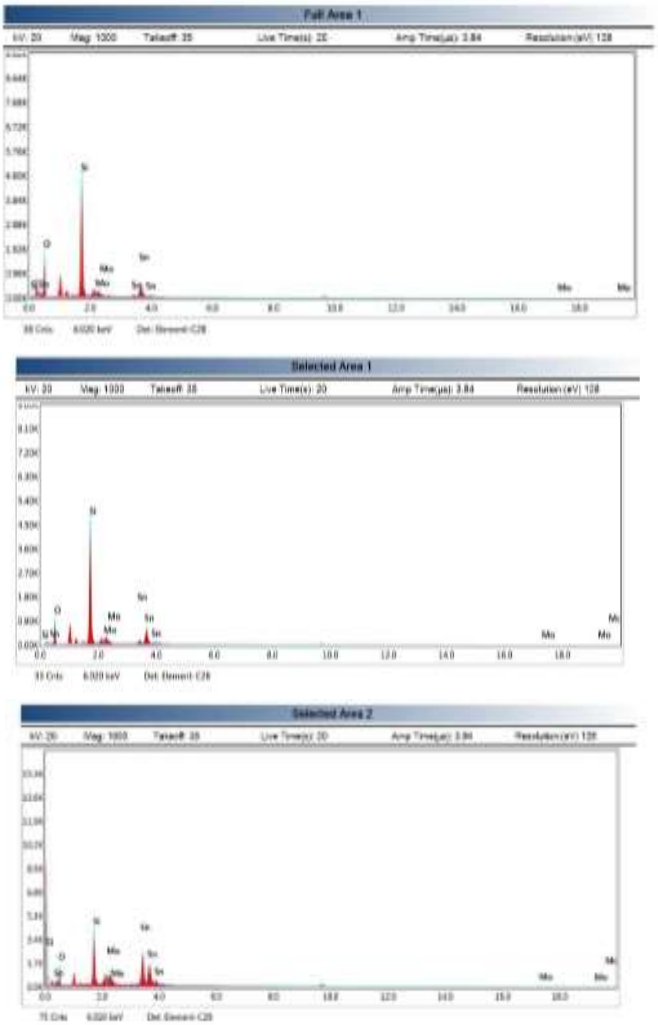

Figure 4. EDX spectrum of MoO_3 doped SnO_2 thin films.

Additionally, this Figure 5a showed that the previously mentioned shoulder was seen to be blue-shifted by increasing MoO_3 dopants ratio to be located near 280 nm for MTDO15 thin film.

Here, a spin -coated thin film was subjected to optical spectroscopic analysis using the transmission method, where the absorption coefficient (α) is given by the Lambert's formula (Tauc et al., 1966)

$$\alpha = 1/t \ln (1/T) \quad (3)$$

Where T and t are transmittance and film thickness, respectively. Using this phrase, it was noticed that for each of the spin-coated thin films, the absorption coefficient (α) had high values (10^4) across the entire spectral range investigated here. Due to These high values, thin films have a lot of potential for use as potential photovoltaic materials (Lin and Lee, 2014).

The spectral distribution of the absorption coefficient near the fundamental edge for a 10^4 (i.e. in the high absorption region) is provided in more general terms by the David and Mott expression (Shkir et al., 2019):

$$\alpha(h\upsilon) = \frac{1}{h\upsilon}[A(h\upsilon - E_g^{opt})^m] \quad (4)$$

Where A is constant is determined by the transition probability, the optical bandgap width is denoted by E_g^{opt} and m is an exponent that describes the optical absorption processes occur within the investigated film sample. Theoretically, m = 1/2, 2, 3/2 or 3 for the direct allowed, indirect allowed, direct forbidden or indirect forbidden transitions, respectively (Gupta et al., 2017) and (Shakir et al., 2009).

The kind of the optical transition within such a thin film sample is typically identified by plotting the quantity $(\alpha h\upsilon)^{(1/m)}$ as a function of the incident photon energy hυ concurrently for the four values of the exponent n mentioned above , yielding a set of four plots.

One of these plot lines shows the broadest linear relationship of the experimental values in the high absorption region, and thus the matched exponent identifies the kind of the optical transition occurring in the film sample.

In the present study, All of spin deposited TDO and MTDO thin films reveal a direct allowed transition as the dominant optical transition, with the broadest linear relationship was shown for a film sample when m=1/2.

As a Consequence, for all of the thin films studied here, the quantity $(\propto h\upsilon)^2$ was plotted as function of the incident photon energy hυ, while the spectral dependence of absorption coefficient α(hυ) was measured throughout the spectral region 190–2700 nm as shown in figure.

These (Figures 5 b, c, d, e and f) showed that all of the TDO and MTDO thin films reveal consistent of the quantity $(\propto h\upsilon)^2$ as a function of photon energy across the entire studied spectral region.

According to this behavior, the quantity $(\propto h\upsilon)^2$ in the high absorption region increases linearly data as photon energy rises. Additionally, Figure 5a showed that as the doping percentage increases, the absorption edge shifts to blue end of the spectrum, reflecting an improvement of the optical bandgap.

The experimental data in the high absorption region were fitted to a linear equation, and the width of the direct allowed bandgap was estimated by extrapolation of a straight line down to $(\propto h\upsilon)^2 = 0$ for the film sample studied here. In the summary table, the estimated bandgap widths were collected and recorded.

This table 2 clearly show that the optical bandgap for TDO film sample was found to be 3.97eV, showing the highest bandgap width. Alongside, by increasing the weight percentage of the MoO_3-

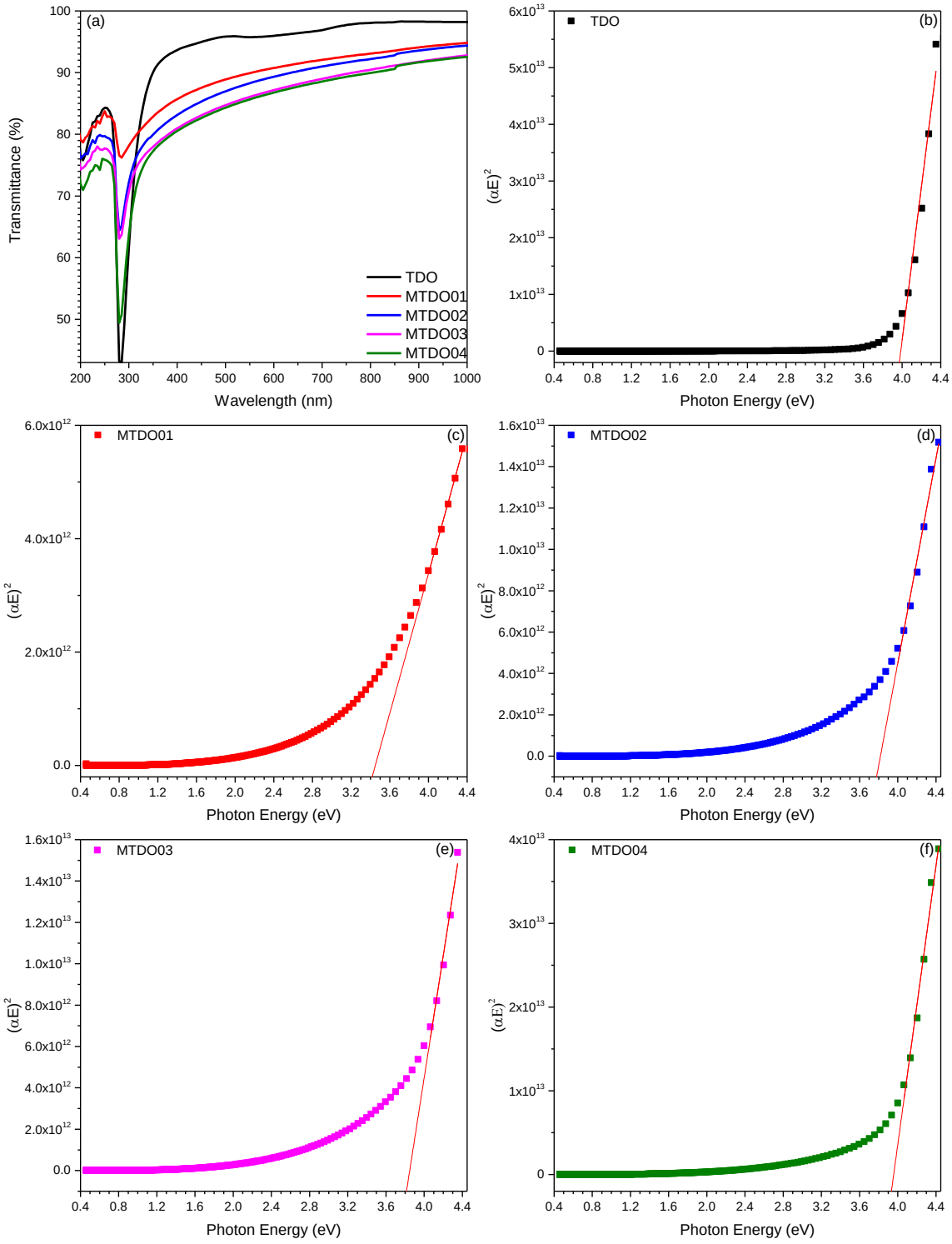

Figure 5. (a) The optical transmission spectra measured at room temperature for pure and MoO_3 doped SnO_2 thin films. (b -f) typical variance of the quantity $(h\upsilon)^2$ as a function of the incident photon energy for pure and MoO_3 doped SnO_2 thin films.

doping content, the optical bandgap was decreased until it reached 3.41 eV for MTDO01 thin film, depicting the lowest bandgap width. Then, the optical bandgap was increased until it reached 3.93 eV for MTDO04 thin film. According to the results in this regard, the TDO00 thin film exhibits an optical bandgap that is significantly larger than the SnO_2 standard bandgap (3.597 eV) (Fröhlich et al., 1978) and (Reimann and Steube, 1998).

Table 2. The values of the optical transmission at a certain wavelength and the direct allowed bandgap for pure and MoO_3 doped SnO_2 thin films.

Thin Film Code	Optical transmission (%)	Direct Optical Band-gap(eV)	FOM Values
TDO	95.95	3.97	1.56×10^{-3}
MTDO01	90.74	3.41	5.11×10^{-5}
MTDO02	89.33	3.78	2.55×10^{-5}
MTDO03	87.16	3.81	2.05×10^{-5}
MTDO04	86.76	3.93	1.33×10^{-5}

The increasing energy band gaps values of TDO and MTD02, MTDO03and MTDO04 may be attributed to the Moss-Burstein (MB) Effect. Whereas the increased carrier concentration brought on by doping shifts energy to the higher levels .This shift occurred as the lowest bands filled as a result of the increased carrier concentration brought on by the MoO_3 doping of SnO_2. These filled bands effectively pushed the electrons excited from the valence band to the higher unoccupied energy levels above these filled levels, increasing the bandgap energy in this work (Burstein, 1954).

The decreasing of optical bandgap value of MTDO01 due to crystal defects (dislocation density and macrostrain) and poor crystallinity (Freund and Suresh, 2004) and (Turgut et al., 2013).

As a result, the bandgap width of MTDO01 thin film is comparable (smaller) to the standard value, whereas the bandgap width of MTDO04 thin film is greater than the standard bandgap of SnO_2.

As previously stated, the experimental results indicated a significant decrease in optical bandgap width followed by an increase in optical bandgap width by increasing the moo3 doping concentration. This is accordance with the notices that have been obtained by (Turgut and Sönmez, 2014) and (Ganesh, et al. 2019) however, the results reported by (El Radaf et al., 2019) and (Mazloom and Ghodsi, 2013) are inconsistent. Comparable optical bandgap values For the TDO and MTDO thin films spin coated with various MoO_3 doping concentration have previously been found in several studies (e.g. (Turgut and Sönmez, 2014) and (Turgut et al.,2014)) . This could be because thin film characteristics are particularly sensitive to the preparation conditions, even done in the same laboratory. As a result, changes in the bandgap width of SnO_2 can be attributed to using of various laboratories or various deposition method when done in the same laboratory (Patil et al., 2011) and (Patil et al., 2012).

Here, increasing the MoO_3 doping concentration results in a noticeable increase in bandgap width of the TDO and MTDO thin films, which is attributed to the improvement in crystallinity and leads to a smaller grain size as deduced from the XRD results. However, a decrease in crystallinity implies an increase in the density of the grain boundaries, which permit the formation of structural crystal defects.

In the main, a verity of factors work together to influence how significantly the bandgap width of the SnO_2 and MoO_3doped SnO_2 film samples change (e.g. crystalline size, carrier concentration, and presence of impurities and defects in the film sample (Mariappan et al., 2014) and (Korber et al., 2008).

3.4. Dc electrical conductivity

Metal oxide semiconductors have a variety of defects, including interstitials, impurities, dislocation, and grain boundaries the main two elements controlling the electrical conductivity of such a metal oxide semiconductor are the carrier concentration and mobility.

The intrinsic point defects, such as oxygen/metal interstitials, oxygen sites occupied by metal ions, and/or oxygen sites occupied by metal ions, are what cause the increase in charge carrier density in a pure MOS material (Paine et al.,1999).

As a result of the presence of extrinsic point defects caused by the inclusion of negative or positive dopants in the host lattice of a metal oxide semiconductor, further increase of carrier concentration and subsequently greater electrical conductivity may be achieved.

(Oshima et al., 2009) have reported that F doped SnO_2 thin films (0 to 5mol %) were deposited on glass substrate at500℃ by spray pyrolysis. Un-doped and doped SnO_2 thin films were all of n-type, indicating that fluorine atoms can act as donor impurities. The lowest resistivity of $1.4 \times (10)^{-3}$ **Ω**.cm was obtained at a fluorine concentration of 4mol %.

Consequently, the presence of intrinsic and/or extrinsic defects together with the metal oxide structure leads to the creation of new occupied or unoccupied states inside the bandgap. These states change the charge carrier density, which improves the conductivity of the p-type or n-type (Lee et al.,1990) and (Ivashchenko et al., 1997).

In the lattice of the majority of pure metal oxides, the metal ions are as positive point charges (Mx^{+--} cation), where x is the formal oxidation state of the transition metal, and the oxygen ions are treated as a negative point charge (O^{2--}anion).

Since there isn't actually a perfectly stoichiometric metal oxide in existence (i.e., one without any defects), and since entropy necessitates the existence of some finite concentration of intrinsic defects, the presence of defects in a crystal structure is a thermodynamic prerequisite for stable structure. The behavior of such a metal oxide is therefore either that of a p- or n-type semiconductors. The electrical resistivity of SnO_2 thin films produced using various processes is significantly less than this value as reported in most previous literature (Stjerna et al., 1994), despite the fact that pure and completely stoichiometric SnO_2 exhibits insulating behavior, representing a resistivity of 10^8**Ω**.cm (Bagheri-Mohagheghi and Shokooh-Saremi, 2004).

For all thin films under research study here, electrical measurements were made in an evacuated medium at working temperatures ranging from 370 to 460K. The electrical resistance for spin-coated TDO and MTDO film samples as a function of temperature. A typical three-dimensional sample's bulk resistance can be represented as:

$$\mathbf{R}=\rho\frac{L}{A}=\boldsymbol{\rho}\left(\frac{L}{wt}\right) \qquad \mathbf{(5)}$$

Where ρ is the sample's electrical resistivity, L is its length, and A is its cross sectional area, which can be divided into the sample's width (w) and sample thickness (t).

The surface resistance, on the other hand, applies to a typical two-dimensional sample such thin films, where the word surface resistance denotes that the current flow is parallel to the sample surface rather than perpendicular to the film sample.

Here, the sample contacts and connections were made sequentially for a TDO and MTDO thin films samples, resulting in the sample's width being equal to its length, while this sample elaboration was done for a sample area encompassing the thicker film one (near the edges of the spin-coated substrate). Therefore, the surface resistance can be estimated using the calculation,

$R_{sur}=\rho_{sur}=$ ρ (1/t) **Ω**/cm^{-1}, where the bulk resistivity is provided as:

$$\boldsymbol{\rho=R\ (A/L) = (V/I)\ (wt/L)\ \Omega.cm.} \qquad \mathbf{(6)}$$

The Figure 6a depicts the change of dc-conductivity as a function of dopant concentration for all the thin films studied. Figure 6a shows that the produced SnO_2 and MoO_3 doped SnO_2

thin films reveal a high dependency of the dc-conductivity on dopant concentration. According to Consequence, this (Figure 6a ,b) indicates that the behavior of the dc conductivity as a function of the dopant concentration is not Obvious enough for the thin films produced at high dopant concentrations.

It can be seen from (Figure 6c, e) that the present raises as the working temperature increases from 370K to 460K, increasing the conductivity from 8.11×10^{-3} to 3.91576 $(\Omega.cm)^{-1}$ for TDO, 2.47286×10^{-4} to 23.08×10^{-3} $(\Omega.cm)^{-1}$ for MTDO01, 1.24014×10^{-4} to11.16×10^{-3} $(\Omega.cm)^{-1}$ for MTDO02, 9.16474×10^{-5} to 11.2×10^{-3} $(\Omega.cm)^{-1}$ for MTDO03, 1.47288×10^{-4} to 12.7×10^{-3} $(\Omega.cm)^{-1}$ for MTDO04.

These studies demonstrated that the dc-conductivity of such a thin film frequently raises by more than one order of magnitude as the working temperature rises from 370k – 460K. Additionally, (Figure 6c, e) indicates a decrease in the dc-conductivity of the obtained thin films with an increase in dopant concentration over the entire operating temperature range (370K– 460 K). The Figure 6a demonstrate that at 460K, the conductivity of the thin film decreases from 3.91576 to 12.7×10^{-3} $(\Omega.cm)^{-1}$ with an increase in the dopant concentration from 0 wt. %-to 15 wt. %.

This behavior is in line with a number of observations that have already been published in the literature (Muranaka and Bando., 1992). However, these results are at variance with the findings that have been reported in various previous studies (Ray et al., 1997).Overall, the spin- deposited film samples under investigation here have electrical conductivity values that are similar to those previously reported in various investigations (Muranaka and Bando., 1992). The electrical conductivity values of MoO_3 doped SnO_2 thin films may explained that the electrical conductivity of spin coated thin films can be decreased by replacing Mo atoms with low valance states with Sn^{4+} ions. Some of the Mo^{6+} ions are reduced to low valence levels in this instance, which results in the formation of acceptor states.

Another reason contributing to the decrease in electrical conductivity for spin-coated thin films may be the excess Mo atoms, which are unable to occupy the necessary lattice positions to provide free carriers and may lead to an increase in disorder levels, which in turn reduce electrical conductivity. Free charge carriers may be interacted in such a polycrystalline TCO thin film by a variety of scattering mechanisms, including thermal lattice vibration, intrinsic and/ or extrinsic defects, however grain boundary scattering is frequently the predominant mechanism in these thin films (Moholkar et al., 2008).

The main scattering mechanisms in TCO thin films are ionized impurities scattering at low temperature and grain boundaries scattering at high temperature (Chopra et al.,1983) and (Thangaraju,2002). The grain boundary is known to possess more defects, impurities, and traps than grain interiors. A semiconducting material's potential transport systems' activation energies are most frequently assessed using the Arrhenius- type relation (Mahmoud et al., 2002) and (Bromberg, 1984)

$$\sigma_{(DC)}(T)=\sigma_{(0)}\ \exp\left(-\frac{\Delta E}{kT}\right) \qquad (7)$$

Where, σ (0) is the pre-exponential factor, ΔE is the thermal activation energy in (eV), T is the temperature in absolute scale and k is the Boltzmann constant. Furthermore, the figure 6d shows that TDO thin film under study demonstrates behavior; namely an exponential increase in dc-conductivity with an increase in the working temperature from 360 K– 460 K, indicating two stages of conductivity.

The conductivity does not vary considerably with increasing temperature over the low temperature region (extrinsic conduction region), in the first stage (360 K– 414K).

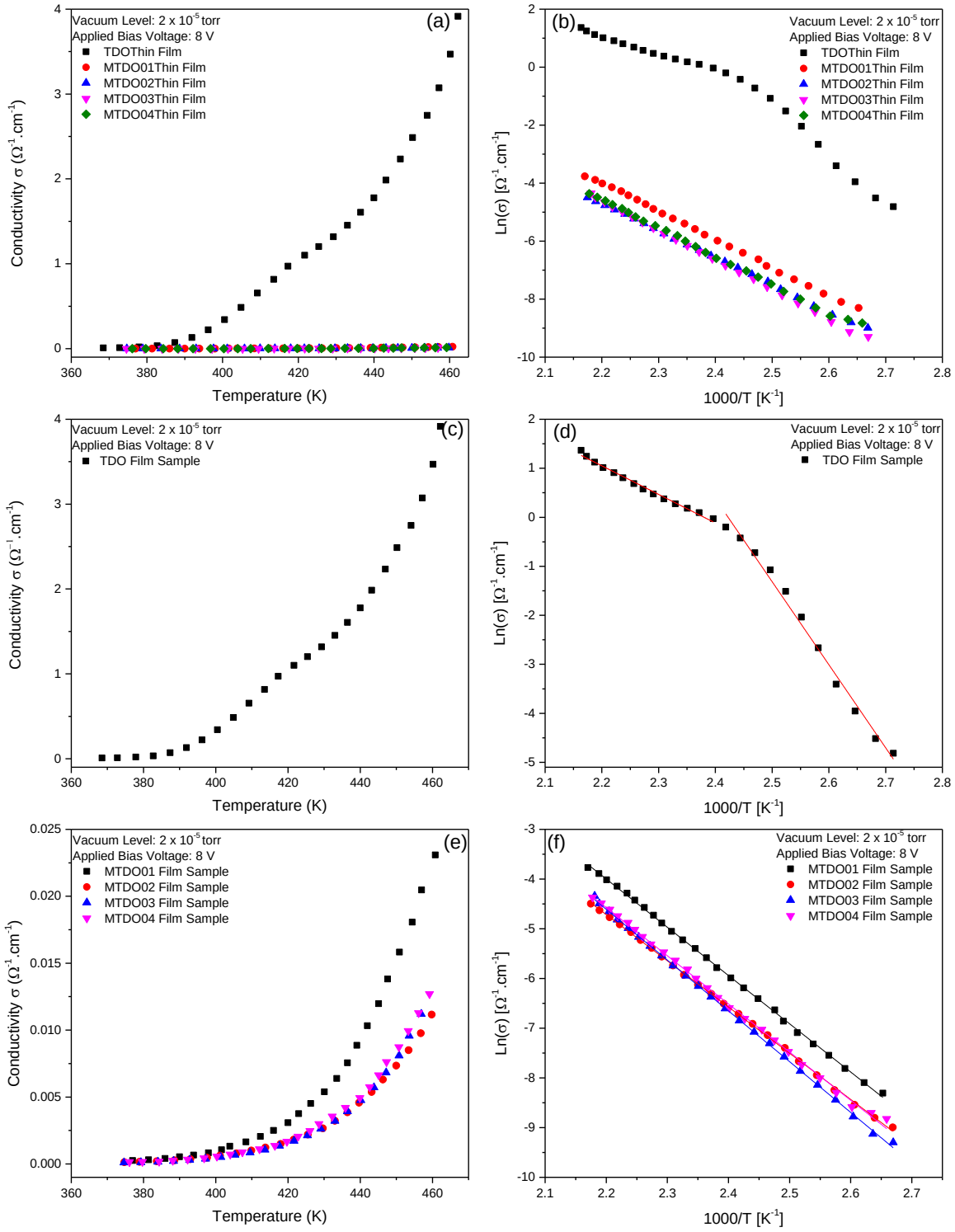

Figure 6. The variation of the DC Electrical conductivity as a function of the working temperature and typical variation of the quantity ln (σ_{DC}) as a function of the reciprocal working temperature for pure and MoO_3 doped SnO_2 thin films.

The dc-conductivity increases rapidly with the rising temperature in the second stage (414 K–460 K) over the high temperature region (intrinsic conduction region). It can be seen figure 6f, The MoO_3 doped SnO_2 thin films under investigation show typical behavior, which is, an exponential increase of the dc-conductivity with an increasing working temperature from 370 K– 460 K (intrinsic conduction region). For such a curve within the plot described in figure

6b, the thermal activation energy was determined based on the slope of the linear fitting to the experimental data.

As the operating temperature raises from 370 K– 460 K, it can be observed that the quantity ln(σ_{dc}) varies linearly with 1000/T showing two varied conduction processes with different activation energies of conductivity for the same un-doped SnO_2 thin film (figure 6d). In the working temperature region of 370 K– 414 K, it is evident from figure that the quantity ln (σ_{dc}) varies linearly with 1000/T in a greater slope for such a pure SnO_2 thin film.

With a further increase in the working temperature up to 460 K (418 – 460K), such a pure SnO_2 thin film exhibits a significant linear variation of the quantity ln (σ_{dc}) varies linearly with 1000/T in a smaller slope for such a pure SnO_2 thin film (figure 6d). This can be assigned to two regions extrinsic and intrinsic conduction processes. The values of the activation energies ΔE1 and ΔE2 were determined for TDO00 thin film under investigation based on the slopes at the operating temperature regions 370K– 414 K and 418K– 460 K, respectively (see Table 3).

Table 3. The values of the Dc Electrical parameters (e.g., $\sigma_{DC}(T)$ and $\Delta E_{DC}(T)$ for pure and MoO_3 Doped SnO_2 thin films.

Thin Film Code	Conductivity Values		Activation Energy	
	AT 370K	370K To 460K	368.5 K To 414.9 K	417.78 K To 455.8 K
TDO	0.00811	3.91576	3.362153428	1.157530193
			370 K To 460 K	
MTDO01	2.4729×10^{-4}	0.02308	1.9267	
MTDO02	1.2401×10^{-4}	0.01116	1.8451	
MTDO03	9.1647×10^{-5}	0.0112	2.0268	
MTDO04	1.4729×10^{-4}	0.0127	1.9232	

These values are in line with the findings that have previously been observed in some works (Joseph t al., 2009).

Even so, as shown in the Figure 6f, the temperature dependence of the dc-electrical conductivity (σ_{dc}) was explored for such a film sample over working temperatures range of 370 K- 460 K.

The values of the activation energy ΔE was estimated for MoO_3 doped SnO_2 thin films under investigation based on the slopes at the operating temperature region 370 K– 460 K, as inferred from Table 3.

The estimated values of ΔE suggest that as the dopant concentration increases from 07wt%-15wt%, the activation energy of the obtained SnO_2 doped MoO_3 thin films decrease from 1.926 eV for the MTDO01 thin film to 1.923eV for the MTDO04 thin film. These values can be assigned to the intrinsic conduction mechanism within SnO_2 doped MoO_3 thin films. These results can be attributed to intrinsic conduction activities identified within the SnO_2 nanocrystals as a result of thermal activation of charge carriers throughout the bandgap width.

Deep donor or acceptor levels, which may have been caused by the intrinsic point defects and impurities, are cause of the decreased thermal activation energy (Patil et al., 2003). The substitution of substantially Mo^{6+} atoms generating deep donor or acceptor levels for Sn^{4+} atoms at cation sites may be reasonable explanation for the decrease in activation energy of MoO_3 doped compared un-doped thin films.

3.5. Figure of merit

The figure of merit is a significant factor to evaluate TDO and MTDO thin films for use in solar cell applications. Tin oxides thin films Electrical Conductivity and optical transmittance are two parameters inversely proportional to each other and should be as high as possible for effective usage.

In the present investigation, the un-doped SnO_2 thin film (TDO thin film) shows the highest conductivity which was found to be decreased by increasing the MoO_3 doping concentration reaching the its lowest value for the MTDO04 thin film. The un-doped SnO_2 thin film (TDO thin film) exhibits the highest optical transmission in the visible region that was found to be reduced by increasing the MoO_3 doping concentration indicate the lowest transparency for the MTDO04 thin film. Therefore, the FOM value characterizes the degree of the film suitability in the practical optoelectronic uses.

The FOM parameter is a conductive tool for measuring the behaviors of several TCO film samples, giving preferable adjustment to solar cell applications. This parameter is defined by Scropp's expression that can be present as: $\varphi = (-1)/(\rho \ln T)$ (Amirtharajan et al., 2016), where ρ is the electrical resistivity for such a thin film in this work, T is the optical transmission at a particular wavelength in the visible region λ=600nm. Figure 7 shows that the FOM value decreases from 1.55×10^{-3} to 1.33×10^{-5} Ω^{-1} by increasing the MoO_3 doping concentration from 0 to 15 wt. %. From these experimental results, the values of the FOM parameter are much smaller than the outcomes that have been observations reported in literature (El Radaf et al., 2019), while the sequence behavior of the FOM value as conclusion of the different in the doping concentration is disagreement with other results reported in some studies (Turgut and Sönmez , 2014) and (Turgut et al., 2014).

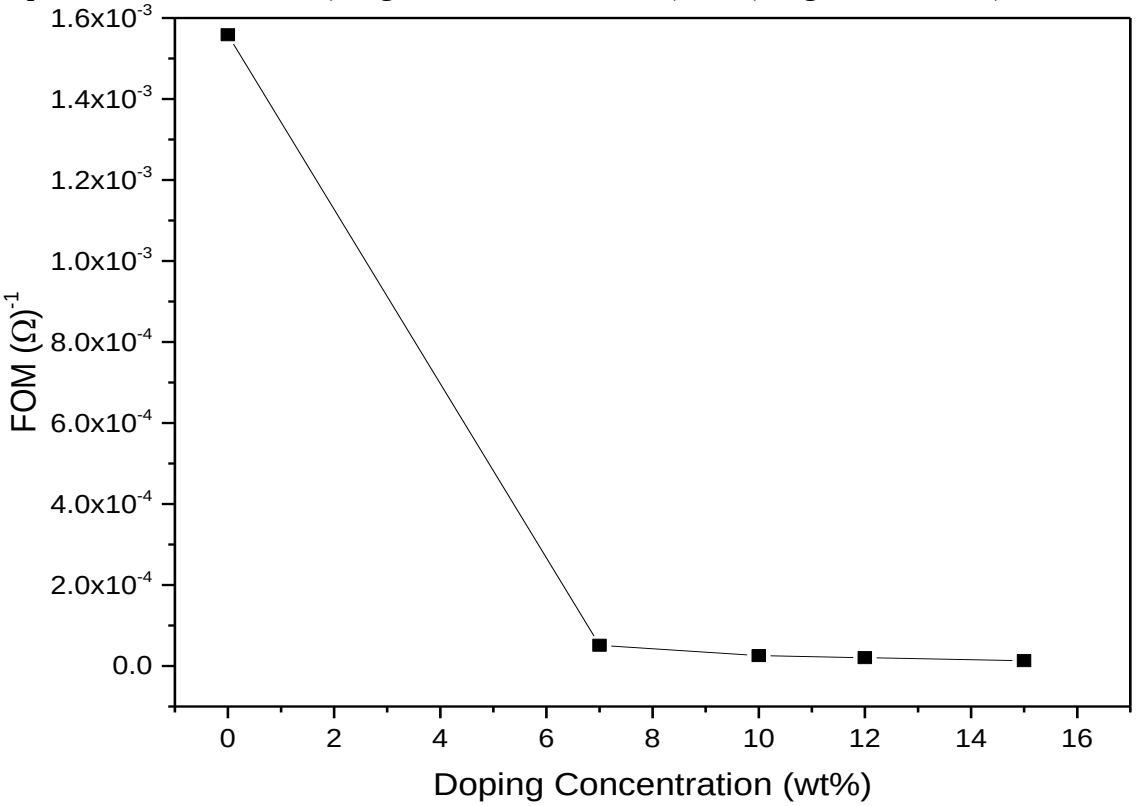

Figure 7. The variation in the highest value of the FOM factor as a function of the doping concentration of MoO_3. The plot shows that the highest FOM factor corresponding a certain wavelength for each pure and MoO_3 doped SnO_2 thin films.

The above-mentioned observations also exhibited all the spin coated film samples have a great potential to be used in optoelectronic applications, and the TDO thin film reveals the best FOM value, and sequence it occupy the preferable optoelectronic properties between all the TDO and MTDO thin films investigated here.

4. Conclusion

Pure and MoO_3 doped SnO_2 thin films are deposited onto glass substrate by spin coating technique. The XRD revealed that the structure TDO and MTDO thin films are tetragonal rutile type structure, MTDO thin films have low intensity peak inferred to stable and metastable phases such orthorhombic and monoclinic. The crystallite size decreased from 74.83 to 48.42 nm with increasing MoO_3 dopant concentration. SEM micrographs also showed that the increment of MoO_3 doping concentration caused reduce on the spherical particle size distributed in the surface from 25.5nm to 9.9 nm. EDX spectra confirmed the successful incorporation of MoO_3 in SnO_2 lattice.

The optical studies reveal that the average visible transmittance decreased by increasing MoO_3 doping concentration from 95.95 for TDO to 86.76 for MTDO04 and thus the great optical transparency noticed in the visible region indicates a possible interest in these coating for particle applications in optoelectronic devices (such as energy efficient windows and solar cells).

The direct optical bandgap decreased from 3.97 eV for TDO film to 3.41eV for MTDO01 film and then increase to 3.94 eV for MTDO04 thin film. The decreasing then the enhancement of the direct optical bandgap may be attributed to crystal defect and smaller crystallite size as inferred from the XRD results. The DC electrical conductivity decreased from 3.91576 for TDO to $12.7\times10^{-3}(\Omega.cm)^{-1}$ for MTDO04 at 460 K by increasing MoO_3 concentration is due to Sn^{4+} Ion by Mo^{6+} Ion which reduces the carrier concentrations. The thermal activation energies for TDO thin film were estimated $\Delta E1$= 3.36 and E2 =1.158 eV but the values of thermal activation energies for MTDO thin films were decreased from 1.926 to 1.923 eV. The highest figure of merit $1.55\times10^{-3}\ \Omega^{-1}$ was obtained for the film prepared at 0 wt. doping level with high transparency at 600nm and low resistivity as a cost effective TCOs film. The obtained values of the optical transmission ,optical bandgap , and conductivity of MoO_3 doped SnO_2 thin films as TCO support the applicability of these films in solar cells applications and optoelectronic devices.

References

Ahmed Sk.F., Khan S., Ghosh P.K., Mitra M.K.and Chattopadhyay K.K., (2006) Effect of Al doping on the conductivity type inversion and electro-optical properties of SnO_2 thin films synthesized by sol-gel technique J. Sol–Gel Sci. Techn. 39, 241–247.

Alenezi M.R., Alzanki T.H., Almeshal A.M., Alshammari A.S., Beliatis M.J., Henley S.J.and Silva S.R.P., (2014) Hierarchically designed ZnO nanostructure-based high performance gas sensors, RSC Adv. 4 (90) 49521–49528.

Ali D., Butt M.Z., Muneer I., Bashir F. and Saleem M, (2017) Correlation between structural and optoelectronic properties of tin-doped indium oxide thin films, Optik 128, 235–246.

Alinauskas L., E. Brooke, Regoutz A., Katelnikovas A., Raudonis R., Yitzchaik S., Payne D.J. and Garskaite E., (2017) Nanostructuring of SnO_2 via solution-based and hard template assisted method, Thin Solid Films 626, 38–45.

Amirtharajan S., Jeyaprakash P., Natarajan J., Natarajan P., (2016) Electrical investigation of TiO_2 thin films coated on glass and silicon substrates—effect of UV and visible light illumination Appl Nanosci 6,591–598.

Arbiol J., Morante J.R., Bouvier P., Pagnier T., Makeeva E.A., Rumyantseva M.N. and Gaskov A.M., (2006) SnO_2/MoO_3-nanostructure and alcohol detection, Sens. Actuators B: Chem. 118,(1-2), 156–162.

Arif M., Monga S., Sanger A., Vilarinho P.M. and Singh A., (2018) Investigation of structural, optical and vibrational properties of highly oriented ZnO thin film, Vacuum 155, 662–666.

Bagheri-Mohagheghi M.M.and Shokooh-Saremi M., (2004) Electrical, Optical and structural properties of Li doped SnO_2 Transparent Conducting Films Deposited by teh Spray pyrolysis technique: A carrier – type conversion Study, Semiconductor Science and Technology, Semicond. Sci. Technol. 19, 764.

Bouaine A., Brihi N., Schmerber G., Ulhaq-Bouillet C., Colis S. and Dinia A., (2007) Structural, optical, and magnetic properties of Co-doped SnO_2 powders synthesized by the coprecipitation technique, J. Phys. Chem. C 111,(7), 2924–2928.

Bromberg J.P., (1984) Physical Chemistry, 2nd Edition Allyn and Bacon, Boston,.

Burstein E., (1954) Anomalous optical absorption limit in InSb Phys. Rev. 93, 632–633.

Chao L., Wei W., Tongchi X., Huanxin W., Youqi Z. and Yanliang S., (2010) La-doped SnO_2 synthesis and its electrochemical property, J. Rare Earths 28 161–163.

Choi Y.-H., Yang M.and Hong S.-H., (2008) H_2 sensing characteristics of highly textured Pd-doped SnO_2 thin films, Sens. Actuators B: Chem. 134, (1), 117–121.

Chopra K.L., Major S. and Pandya D.K., (1983) Transparent conductors –a status review, Thin Solid Films 102,(1),1-46.

Cullity B D and Stock S R (2001) Elements of X-Ray Diffraction 3rd edition (New York: Prentice-Hall Inc) pp 167–71 0-201-61091-4

El Radaf I.M, Hameed T A, Elkom G.M and Dahy T.M, (2019) Synthesis, structural, linear and nonlinear optical properties of chromium doped SnO_2 thin films, Ceramics International 45, (3), 3072–3080.

Fan J., Li T.and Heng H., (2014) Hydrothermal growth and optical properties of ZnO nanoflowers, Mater. Res. Express 1, (4), 045024.

Freund L.B and Suresh S., (2004) Thin Film Materials: Stress, Defect Formation and Surface Evolution, Cambridge University Press, p. 192.

Fröhlich D., Kenklies R. and Helbig R., (1978) Band-gap assignment in SnO_2 by two-photon spectroscopy, Phys. Rev. Lett. 41, (25), 1750–1751.

Ganesh V., Arif M., Manthrammel M.A, shkir M., Singh A. and AlFaify S (2019) Effect of La doping on key characteristics of SnO_2 thin films facilely fabricated by spin coating technique Optical Materials 94 , 277–285.

Givargizov E.I., (2013) Oriented Crystallization on Amorphous Substrate, Plenum Press, New York, (Chapter 4).

Gupta V., Sharma N., Singh U., Arif M. and Singh A., (2017) Higher oxidation level in graphene oxide, Optik, 143,115–124.

Ibrahim N.B., Abdi M.H., Abdullah M.H. and Baqiah H., (2013) Structural and optical characterization of undoped and chromium doped tin oxide prepared by sol–gel method, Appl. Surf. Sci. 271, 260–264.

Ivanovskaya M., Bogdanov P., Faglia G., Nelli P., Sberveglieri G. and Taroni A., (2001) On the role of catalytic additives in gas–sensitivity of SnO_2-MO based thin film sensors, Sensors Actuators B 77,(1-2), 268–274.

Ivashchenko A. I., Kerner Ia. I., Kiosse G. A., and Maronchuk I. Yu., (1997) Dimensional effect on the electrical conductivity of polycrystalline SnO_2 thin films ,Thin Solid Films 303,(1-2), 292-294.

Joseph D.P., Renugambal P., Saravanan M., Raja S. P., Venkateswaran C., (2009) Effect of Li doping on the structural, optical and electrical properties of spray Deposited SnO_2 thin films, Thin Solid Films 517,(21), 6129–6136

Kaplan L., Zhitomirsky V.N., Goldsmith S., Boxman R.L. and Rusman I., (1995) Arc behaviour during filtered vacuum arc deposition of Sn–O thin films, Surf. Coat. Technol. 76–77, 181–189.

Korber C., Harvey S.P., Mason T.O., and Klein A., (2008) Barrier heights at the SnO_2/Pt interface: in situ photoemission and electrical properties, Surf. Sci. 602, (21), 3246 – 3252.

Krishnapriya R., Praneetha S.and Murugan A. V., (2015) Energy-efficient, microwave assisted hydro/solvothermal synthesis of hierarchical flowers and rice grain-like ZnO nanocrystals as photoanodes for high performance dye-sensitized solar cells, CrystEngComm 17,(43), 8353–8367.

Lee J. H., Park S. J. and Hirota K.,(1990) Temperature Dependence of Electrical Conductivity in polycrystalline Tin Oxide J. Am. Ceram.Soc. 73,(9), 2771.

Lin Y-C. and Lee M-W., (2014) Bi2S3 Liquid-Junction Semiconductor-Sensitized SnO_2 Solar Cells ,Journal of The Electrochemical Society, 161 (1) H1 .

Liu S.-J., Chen L.-Y., Liu C.-Y., Fang, H.-W., Hsie J.-H., Juang J.-Y., (2011) Physical properties of polycrystalline Cr-doped SnO_2 films grown on glasses using reactive dc magnetron co-sputtering technique, Appl. Surf. Sci. 257, (6), 2254–2258.

Lu Y-J., Shan C-X., Jiang M-M., Li B-H., Liu K-W., Li R-G.and Shen D-Z., (2014) Enhanced emission from ZnO-based double heterostructure light-emitting devices using a distributed Bragg reflector, RSC Adv. 4,(32), 16578–16582.

Mahmoud S.A., Akl A.A., Kamal H., Abdel Hady K., (2002) Opto-structural, electrical and electrochromic properties of crystalline nickel oxide thin films prepared by spray pyrolysis ,Physica B: Condensed Matter 311,(3-4), 366-375.

Mariappan R., Ponnuswamy V., Suresh P., Ashok N., Jayamurugan P. and Bose A. C., (2014) Influence of film thickness on the properties of sprayed ZnO thin films for gas sensor applications, Superlattices Microstruct. 71, 238–249.

Mazloom J. and Ghodsi F.E., (2013) Spectroscopic, microscopic, and electrical characterization of nanostructured SnO_2: Co thin films prepared by sol–gel spin coating technique, Materials Research Bulletin 48, (4), 1468–1476.

Moholkar A.V., Pawar S.M., Rajpure K.Y. and Bhosale C.H., (2008) Effect of concentration of $SnCl_4$ on sprayed fluorine doped tin Oxide thin films, J. Alloys Compd. 455,(1-2), 440-446.

Muranaka S. and Bando Y., (1992) Reactive Deposition of W-, MO-, and V- doped SnO_2 Films, Bull. Instit. Chem. Res., Kyoto Univ. 70 ,(4), 430–434.

Oshima M., Takemoto Y., and Yoshino K.: (2009) Optical and electrical characterization of FTO films grown by spray pyrolysis method Phys. Status Solidi C 6, (5), 1124-1126.

Paine D. C., Whiston T., Janiac D. , Bersford R., Yang C. O., and Lewis B., (1999) A study of low temperature crystallization of amorphous thin film indium- tin-oxide, J. Appl. Phys. 85, 8445.

Pan J. H., Chai S.Y., Lee C., Park S.-E. and Lee W.I., (2007) Controlled formation of highly crystallized cubic and hexagonal mesoporous SnO_2 thin films, J. Phys. Chem. C 111,(15), 5582–5587.

Park S.-M., Ikegami T. and Ebihara K., (2006) Effects of substrate temperature on the properties of Ga-doped ZnO by pulsed laser deposition, Thin Solid Films 513,(1-2), 90–94.

Patil G. E., Kajale D. D., Ahire P. T., Chavan D. N., Pawar N. K., Shinde S. D., Gaikwad V. B. and Jain G. H., (2011)Synthesis, characterization of SnO_2 thin films prepared by spray pyrolysis Bull. Mater. Sci. 34, (1), 1-9,

Patil G. E., Kajale D. D., Gaikwad V. B. and Jain, G. H. (2012) Effect of Thickness on Nanostructured SnO_2 Thin Films by Spray Pyrolysis as Highly Sensitive H_2S Gas Sensor, Int. J. Nanosci and Nanotech.12, (8), 6192-9201.

Patil P.S., Kawar R.K., Seth T., Amalnerkar D.P. and Chigare P.S., (2003) Effect of substrate temperature om structural , electrical and optical properties of sprayed tin oxide (SnO_2) thin films Ceram. Int. 29 (7)725-734.

Ravichandran K., Thirumurugan K., Begum N. J. and Snega S., (2013) Investigation of P-type SnO2: Zn films deposited using a simplified spray pyrolysis technique, Superlatt. Mic. Struct. 60, 327–335.

Ray S.C., Karanjai M.K. and Dasgupta D., (1997) preparation and study of doped and undoped tin dioxide films by the open air chemical vapor deposition technique, Thin Solid Films 307, 221–227.

Reimann K. and Steube M., (1998) Experimental determination of the electronic band structure of SnO_2, Solid State Commun. 105, (10), 649–652.

Shakir M., Singh B., Gaur R., Kumar B., Bhagavannarayana G.and Wahab M., (2009) Dielectric behaviour and ac electrical conductivity analysis of ZnSe chalcogenide nanoparticles, Chalcogenide Lett. 6 ,(12), 655–660.

Shkir M., M.T. Khan and AlFaify S., (2019) Novel Nd-doping effect on structural, morphological, optical, and electrical properties of facilely fabricated PbI2 thin films applicable to optoelectronic devices, Appl. Nanosci., 9,1417-1426.

Soitah T.N., Yang C. and Sun L., (2010) Structural, Optical and electrical properties of Fe-doped SnO_2 fabricated by sol- gel dip coating technique , Mater. Sci. Semicond. Process. 13, 125–131.

Stjerna B., Olsson E. and Granquist C.G., (1994) Optical and electrical properties of radio frequency sputtered tin oxide films doped with oxygen vacancies, F,Sb,or Mo J. Appl. Phys. 76 3797-3817.

Sun J. Q., Wang J.S., Wu X.C., Zhang G.S., Wei J.Y., Zhang S.Q., Li H. and Chen D.R., (2006) Novel method for high-yield synthesis of rutile SnO_2 nanorods by oriented aggregation, Cryst. Growth Des. 6, (7) 1584–1587.

Tauc J., Grigorovici R. and Vancu A., (1966) Optical properties and electronic structure of amorphous germanium, Phys. Status Solidi B 15,(2), 627–637.

Thangaraju B., (2002) structural and electrical studies on highly conducting spray deposited fluorine and antimony doped SnO_2 thin films from $SnCl_2$ precursor, Thin Solid Films 402,(1-2), 71-78

Turgut G., and Sönmez E., (2014) Synthesis and characterization of Mo doped SnO_2 thin films with spray pyrolysis, Superlattices and Microstructures 69, 175–186.

Turgut G., Keskenler E.F., Aydın S., Sonmez E., Dogan S., Duzgun B. and Ertugrul M., (2013) Effect of Nb doping on structural, electrical and optical properties of spray deposited SnO_2 thin films Superlatt. Mic. Struct. 56 (2013) 107–116.

Turgut G., Sonmez E., Aydin S., Dilber R., Turgut U., (2014) The effect of Mo and F double doping on structural, morphological, Electrical and optical properties of spray deposited SnO_2 thin films Ceramics International40,(8), 12891–12898

Wen Z., Wang G., Lu W., Wang Q., Zhang Q. and Li J., (2007) Enhanced photocatalytic properties of mesoporous SnO_2 induced by low concentration ZnO doping, Cryst. Growth Des. 7 (9) 1722–1725.

Zampiceni E., Bontempi E., Sberveglieri G. and Depero L.E., (2002) Mo influence on SnO_2 thin films properties, Thin Solid Films 418,(1), 16–20.

Zhang Y., Ding F., Deng C., Zhen S., Li X., Xue Y., Yan Y.-M. and Sun K., (2015) Crystal plane-dependent electrocatalytic activity of Co_3O_4 toward oxygen evolution reaction, Catal. Commun. 67, 78–82.